von Karman correlation similarity in solar wind magnetohydrodynamic turbulence

Sohom Roy
Department of Physics and Astronomy, University of Delaware, Newark, Delaware 19716, USA

R. Chhiber
Department of Physics and Astronomy, University of Delaware, Newark, Delaware 19716, USA and Heliophysics Science Division, NASA Goddard Space Flight Center, Greenbelt, Maryland 20771, USA

S. Dasso
CONICET, Universidad de Buenos Aires, Instituto de Astronomía y Física del Espacio, LAMP Group, CC. 67, Sucursal 28, 1428 Buenos Aires, Argentina and Facultad de Ciencias Exactas y Naturales, Departamento de Ciencias de la Atmósfera y los Océanos and Departmento de Física, LAMP Group, Universidad de Buenos Aires, 1428 Buenos Aires, Argentina

M. E. Ruiz
Servicio Meteorológico Nacional, Avenida Dorrego 4019, C1425GBE Buenos Aires, Ciudad Autónoma de Buenos Aires, Argentina and Instituto de Astronomía y Física del Espacio (IAFE) and Departamento de Física, Facultad de Ciencias Exactas y Naturales, Universidad de Buenos Aires, Buenos Aires, Argentina

W. H. Matthaeus
Bartol Research Institute, Department of Physics and Astronomy, University of Delaware, Newark, Delaware 19716, USA

(Received 19 February 2021; revised 17 September 2021; accepted 8 March 2022; published 12 April 2022)

A major development underlying hydrodynamic turbulence theory is the similarity decay hypothesis due to von Karman and Howarth, here extended empirically to plasma turbulence in the solar wind. In similarity decay the second-order correlation experiences a continuous transformation based on a universal functional form and a rescaling of energy and characteristic length. Solar wind turbulence follows many principles adapted from classical fluid turbulence, but previously this similarity property has not been examined explicitly. Here, we analyze an ensemble of Elsässer autocorrelation functions computed from Advanced Composition Explorer data at 1 astronomical unit (AU), and demonstrate explicitly that the two-point correlation functions undergo a collapse to a similarity form of the type anticipated from von Karman's hypothesis applied to weakly compressive magnetohydrodynamic turbulence. This provides a firm empirical basis for employing the similarity decay hypothesis to the Elsässer correlations that represent the incompressive turbulence cascade. This approach is of substantial utility in space turbulence data analysis, and for adopting von Karman-type heating rates in global and subgrid-scale dynamical modeling.

DOI: 10.1103/PhysRevE.105.045204

I. INTRODUCTION

Several fundamental elements of turbulence theory emerge from the von Karman–Howarth treatment of turbulent energy decay in hydrodynamics [1]. A prominent step is the development of equations for the time evolution of second-order (two-point, single-time) correlation functions. These von Karman–Howarth equations are the first in the hierarchy of moment equations and form the basis of the famous Kolmogorov "4/5" law for evaluating the energy cascade rate [2]. An important concept introduced in the same work is that of *self-preservation* of two-point correlations during decay. The conjecture is that the evolution of the correlation functions over an intermediate range of spatial separations ("lags") depends on just a few similarity variables; for hydrodynamics these are two: energy per unit mass u^2, and a single similarity length scale λ. Normalized appropriately, the underlying dimensionless correlation function assumes a quasiuniversal form over the relevant range of length scales. This formalism then implies a familiar decay law for the energy-containing eddies, setting the stage for control of the entire turbulence cascade by the large-scale dynamics. Experimental confirmation of this picture is a cornerstone of hydrodynamic turbulence theory [3–7].

The scope of applications of the von Karman–Howarth ideas extends further, and has been expounded for magnetohydrodynamics (MHD) and for plasmas with support mainly from numerical simulations [8–10]. There is a strong motivation to extrapolate the von Karman approach to observations of turbulence in natural systems. The solar wind offers an effective setting for such studies in a weakly collisional plasma. The fluctuation velocity field $\mathbf{v}$ is important in solar wind

dynamics and is, roughly speaking, in energy equipartition with the magnetic field fluctuations **b**. In classical hydrodynamics, the Reynolds number characterizes turbulent flows. In the solar wind, however, the kinematic viscosity is not well defined, so an effective Reynolds number has been proposed, $\mathrm{Re} = (L/d_i)^{4/3}$ [11], where L is the outer (correlation) scale and d_i is the ion inertial length. This is found to be $\approx 10^6$ at 1 astronomical unit (AU), which lends credence to the likely utility of a turbulence similarity hypothesis in the solar wind. Here, we evaluate directly the self-preservation hypothesis for Elsässer autocorrelation functions observed at 1 AU in the turbulent solar wind. This test employs a large ensemble of samples of solar wind magnetic field and velocity data of sufficient size. These are combined to form the ± Elsässer fields, for which the correlation lengths and energy densities are then computed for each sample. Carrying out the two-stage normalization prescribed in the von Karman procedure, we find a collapse of the correlation functions to a well-defined form. This provides a direct confirmation of von Karman similarity for an extraterrestrial space plasma. This result confirms the quasiuniversality of the correlation functions and associated spectra, an explicit result here, and provides justification for the use of specific model spectral functions in scattering transport theories for solar energetic particles and cosmic rays [12]. Confirmation of the self-preservation property also justifies the use of the MHD von Karman decay/heating rates as essential elements in the macroscopic MHD modeling of plasma behavior in the heliosphere and elsewhere [13–15].

II. VON KARMAN NORMALIZATION

For simplicity and to make contact with theory, we assume that the solar wind magnetic field can be expressed as the sum of the mean magnetic field, and a fluctuation term,

$$\mathbf{B}(\mathbf{x}, t) = \overline{\mathbf{B}}(\mathbf{x}, t) + \mathbf{b}(\mathbf{x}, t), \tag{1}$$

where $\overline{\mathbf{B}}(\mathbf{x}, t)$ is the mean magnetic field, and $\mathbf{b}(\mathbf{x}, t)$ is the fluctuation in the magnetic field. An ensemble average $\langle \cdots \rangle$ defines this decomposition as $\langle \mathbf{B} \rangle = \overline{\mathbf{B}}$ and $\langle \mathbf{b} \rangle = 0$. Similarly, the velocity field **V** is decomposed into mean and fluctuation parts such that $\mathbf{v} = \mathbf{V} - \langle \mathbf{V} \rangle$.

To formulate the von Karman similarity assumption in terms of Elsässer variables and associated energies [16], the magnetic field is converted to Alfvén speed units as $\mathbf{B} \to \mathbf{B}/\sqrt{4\pi\rho}$, where ρ is a suitably coarse-grained mass density (see Ref. [17]). Then define $\mathbf{z}^{\pm} = \mathbf{v} \pm \mathbf{b}$. The incompressible MHD equations in terms of these variables are $\partial_t z_i^{\pm} = -(z_k^{\mp} \mp B_{0k})\partial_k z_i^{\pm} - \partial_i P + \nu \partial_k \partial_k z_i^{\pm}$, where P is the pressure, ν is the viscosity (with equal resistivity), and B_0 is the mean magnetic field in Alfvén units [18].

In the approximation of incompressible turbulence the fluctuation energy density (per unit mass), kinetic plus magnetic, varies in time as $E(t) = u^2(t) + v_A^2(t)$, where $u^2 = \langle |\mathbf{v}|^2 \rangle$ and $v_A^2 = \langle |\mathbf{b}(t)|^2 \rangle$.

The two-point, single-time correlation functions of the ± Elsässer variables are defined as

$$R_{\pm}(\mathbf{r}, t) = \langle \mathbf{z}^{\pm}(\mathbf{x}, t) \cdot \mathbf{z}^{\pm}(\mathbf{x} + \mathbf{r}, t) \rangle. \tag{2}$$

Homogeneity implies that this quantity depends only on the spatial lag **r** and is independent of **x** [6,19]. Note that here we are not assuming stationarity in time, as we are considering turbulence that freely decays in time t. The associated systematic time variation is described by the von Karman hypothesis outlined below. The present theoretical discussion is readily generalized to correlation tensors $R_{ij}^{\pm}(\mathbf{r})$; we forgo this generalization here for brevity. A familiar assumption [1] is that of statistical isotropy, that is, invariance of the correlations under rotations, so that R depends only on the magnitude r of the spatial lag **r**. Alternatively, the theory may be generalized for anisotropic cases [18] (as expected for the solar wind) by introducing length scales parallel and perpendicular to the magnetic field direction. Here, we adopt an ensemble that includes samples for all available directions; by broadening the averaging procedure to sum over all directions, we arrive at a functional representation that is "omnidirectional" [6] and depends on a single spatial lag.

The von Karman similarity in hydrodynamics is based on a single time-varying characteristic length $L(t)$, often associated with the turbulence correlation scale, and a characteristic time $\tau(t) = L(t)/u(t)$. There are at least two potential implications of adopting $L(t)$ and $\tau(t)$ as similarity variables: First, during free decay the semiuniversal solutions can be written that do not involve the laboratory time or length, but only the dimensionless variables t/τ and r/L. The realizability constraints for this *similarity solution* are the von Karman decay laws

$$\frac{du^2}{dt} = -\alpha \frac{u^3}{L}, \quad \frac{dL}{dt} = \beta u. \tag{3}$$

These are quite well established for hydrodynamics [1,2,6] and, by extension, for MHD [8,10]. There is some numerical support for application to weakly collisional plasmas [9].

In MHD, the von Karman hypothesis may be generalized to include two fields $z^{\pm}$, two corresponding length scales $L_{\pm}$ and associated constants $\alpha_{\pm}$ and $\beta_{\pm}$. If such solutions are realized, then the correlation functions themselves undergo a continuous time-dependent renormalization with respect to these variables. Below we verify the approximate validity of this *self-preservation* property for the Elsässer fields [20].

To be specific, the von Karman–MHD similarity hypothesis asserts that the functional form of the two-point Elsässer correlation function is *self-preserving* in the sense that at any stage of the decay,

$$R_{\pm}(r, t) = Z_{\pm}^2(t) \hat{R}^{\pm}(r/L_{\pm}(t)). \tag{4}$$

where $Z_{\pm}^2(t) = R_{\pm}(0, t)$, and $\hat{R}^{\pm}(0) = 1$. Here, $\hat{R}^{\pm}$ are universal functions that describe the dynamics of the two energylike correlation functions over a range of scales r that is much larger than the dissipative scales, and smaller than any specific structures at scales associated with injection of energy. If the hypothesis in Eq. (4) is valid, then an ensemble of realizations of turbulence at various stages of decay would collapse to this form upon adequate averaging over intervals, assuming a standard ergodic property. There is, of course, no guarantee that physically realizable correlation functions will collapse to this form upon appropriate normalization. This must be established empirically. We proceed below to test this approximate collapse to a near-universal form using velocity and magnetic field data at 1 AU. In addition to assessing the quality of the von Karman normalizations for the correlation functions, we carry out the analogous procedure for the second-order

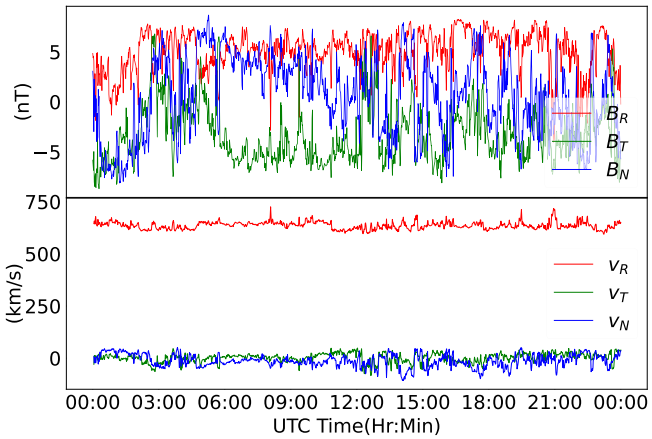

FIG. 1. Top: Magnetic field components in units of nT. Bottom: Velocity components in units of km s^{-1} for the interval 23 January 2003 to 24 January 2003.

Elsässer structure functions,

$$S^{(2)}_{\pm}(\mathbf{r},t) = \langle [\mathbf{z}^{\pm}(\mathbf{x}+\mathbf{r},t) - \mathbf{z}^{\pm}(\mathbf{x},t)]^2 \rangle, \tag{5}$$

a quantity that occupies a prominent role in Kolmogorov's seminal theories [2,7,21,22]. Following Eq. (4) the normalized second-order structure function, assuming isotropy or direction averaging, may be written as

$$S^{(2)}_{\pm}(r,t) = u^2(t)\hat{S}_{\pm}(r/L(t)). \tag{6}$$

III. DATA AND ANALYSIS PROCEDURE

Ensemble of data at 1 AU

The magnetic field values are obtained from Advanced Composition Explorer (ACE) Level 2 MAG (Magnetometer) data [23] at 1-s resolution, which were then downsampled to 1-min cadence. We use the ion velocities from ACE Level 2 Solar Wind Electron Proton Alpha Monitor (SWEPAM) data at 64-s resolution, which is then upsampled to 1-min cadence. The data span 10 years, from 5 February 1998 to 30 March 2008, separated into 1-day intervals, in total comprising approximately 3000 samples after discarding cases that included excessive missing data or bad values. Data sets were cleaned, replacing missing or bad data points with NaN values. The present analysis is restricted to fast wind samples which we define to be those with average wind speeds >500 km/s; this reduced the ensemble to 987 samples. One of these intervals is shown in Fig. 1, which shows the magnetic field and velocity components for the interval 23 January 2003–24 January 2003. The correlation functions are estimated from each data set using the *Blackman-Tukey* algorithm [24], implemented as follows:

Step 1. The magnetic and velocity data for each interval are combined to form Elsasser variables $\boldsymbol{\mathcal{Z}}^{\pm} = \mathbf{V} \pm \mathbf{B}$ with components $\mathcal{Z}^{\pm}_i$ $(i = 1, 2, 3)$. For a given lag τ, two arrays are created, $\boldsymbol{\mathcal{Z}}^{\pm}_{\rm l}$ (the *left* array) and $\boldsymbol{\mathcal{Z}}^{\pm}_{\rm r}$ (the *right* array) for each component and for each field ($\mathcal{Z}^{+}$ and $\mathcal{Z}^{-}$), which are defined as $\mathcal{Z}^{\pm}_{i,\rm l} = \mathcal{Z}^{\pm}_i[0 : L-\tau]$, $\mathcal{Z}^{\pm}_{i,\rm r} = \mathcal{Z}^{\pm}_i[\tau : L]$, where L is the length of the data sample. i takes on values R, T, and N, representing a Sun-centered coordinate system [25].

TABLE I. Standard deviations scaled as $\sigma/R(0)$, for different stages of normalization of the Elsässer variables z_+ and z_- at chosen values of lags.

	Normalization	$r/\lambda = 0.25$	$r/\lambda = 0.5$	$r/\lambda = 1$
z_+	None	1.410	1.318	1.169
	1st	0.165	0.191	0.199
	2nd	0.056	0.042	0.101
z_-	None	1.06	0.975	0.838
	1st	0.174	0.198	0.204
	2nd	0.054	0.043	0.097

Step 2. The correlation tensor for the given lag is computed as $R^{\pm}_{ij}(\tau) = \langle \mathcal{Z}^{\pm}_{i,\rm l} \mathcal{Z}^{\pm}_{j,\rm r} \rangle - \langle \mathcal{Z}^{\pm}_{i,\rm l} \rangle \langle \mathcal{Z}^{\pm}_{j,\rm r} \rangle$, where $\langle M \rangle$ denotes averaging over the entire length of the array M.

Step 3. The full autocorrelation is computed as $R_{\pm}(\tau) = R^{\pm}_{RR}(\tau) + R^{\pm}_{TT}(\tau) + R^{\pm}_{NN}(\tau)$.

Step 4. Time lags are converted to spatial lags using the Taylor frozen-in hypothesis $r = V_{\rm sw}\tau$, where $V_{\rm sw}$ is the solar wind speed for interval I, and r is a spatial lag in the radial direction.

We proceed to apply the normalizations described by Eq. (4) to the collected intervals. Operationally, we compute the correlation lengths $\lambda_{\pm,I}$ and magnetic energy per unit mass $u^2_{\pm,I}$ for each sampled interval. Each correlation function (labeled by interval I) is self-normalized as $R_{\pm,I}(r/\lambda_{\pm,I})/R_{\pm,I}(0)$. Then these are averaged over I to obtain an estimate of the quasiuniversal $\hat{R}_{\pm}(r/\lambda_{\pm})$. The average correlations are compared with the individually normalized correlations in the figures. Note that a median is used to represent the average at each lag.

IV. NORMALIZATIONS AND RESULTS

A. Correlation functions

The top panels of Figs. 2 and 3 illustrate the range of unnormalized correlation functions as a function of unnormalized spatial lag in km. We have used box plots to illustrate the distribution of the correlation functions at each stage in the normalization procedure. The solid line shows the median of the correlation functions at each (binned) lag, and the upper and lower boundaries of the boxes describe the first (Q1) and the third (Q3) quartiles. The whiskers of the box plot show the "minimum" and "maximum" values of the correlations, which are defined with respect to the interquartile range, IQR = (Q3 − Q1), min = Q1 − 1.5 ∗ IQR, max = Q3 + 1.5 ∗ IQR. A measure of the statistical spread of values at a given lag is given as $\sigma/R_{\pm}(0)$, where $R_{\pm}(0)$ is taken from the average $R_{\pm,I}(0)$ in the unnormalized case, and is entered for three values of lag in the first row of Table I. Comparisons are discussed below. It is clear however that the spread of measured correlations (σ) for the unnormalized case is at least several times the average corresponding correlation value for the lags shown in Table I.

The first normalization is accomplished by the procedure $R_{\pm,I}(r) \to R_{\pm,I}(r)/R_{\pm,I}(0)$ for each interval labeled by I. The correlation functions are interpolated onto a uniform grid. The median is then computed for the ensemble of correlation

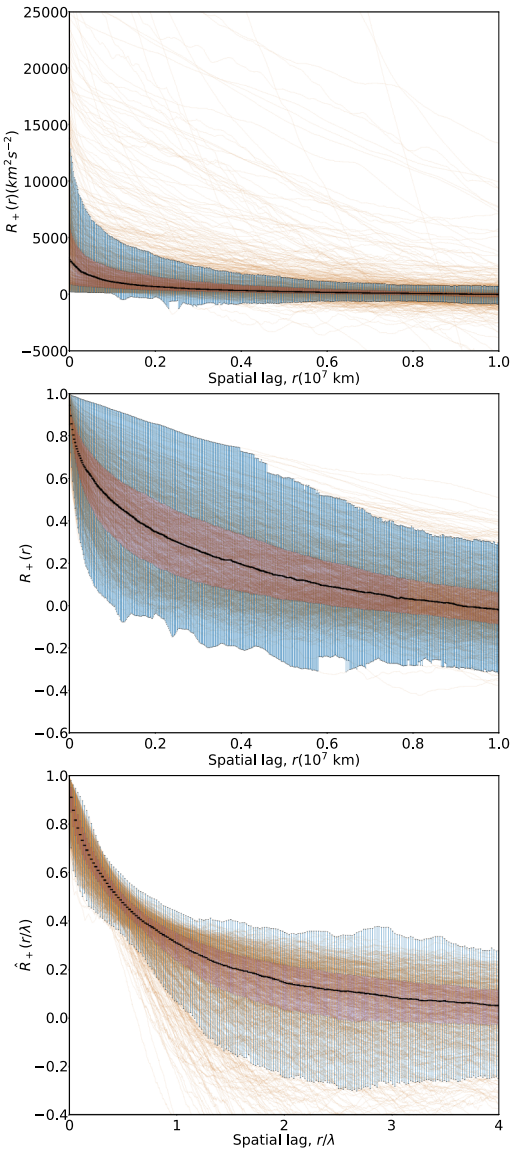

FIG. 2. Top: Unnormalized correlation functions. Middle: First (energy) normalized z^+ correlation function. Bottom: z^+ correlation functions after second normalization (by energy and correlation scale). The solid black line shows median correlation vs lag. The upper/lower boundaries of brown (blue) boxes indicate first (third) quartiles, at each value. "Whiskers" denote the "minimum" and "maximum" values (see text). For these box plots data are interpolated and resampled onto grid of 48 points per 10^6 km span of lag.

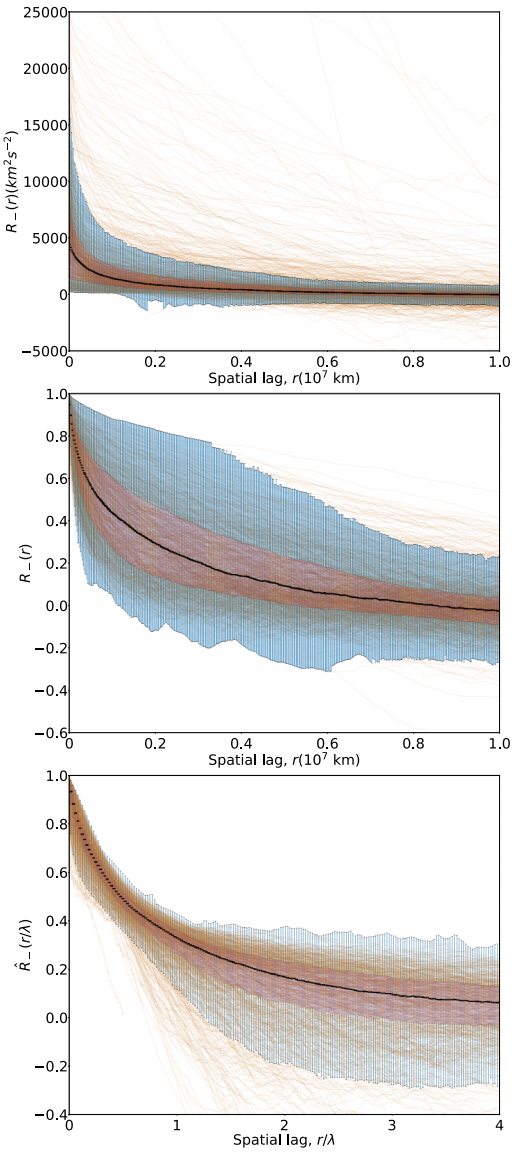

FIG. 3. Top: Correlation functions of z^- not normalized. Middle: Correlation functions of z^- after first normalization—normalization by energy. Bottom: Correlation functions of z^- after second normalization—normalization by energy and correlation scale. Same format as in Fig. 2.

functions at each grid point, along with the "minimum" and "maximum" values as described above. The result, which we call the first-normalized correlation function, is plotted in the middle panels of Figs. 2 and 3 as the median value. The boxes give us an estimate of the spread in the population of $R_{\pm,I}(r)/R_{\pm,I}(0)$ values.

The next step is to compute correlation scales $\lambda_{\pm,I}$ for each sample. The method employed is a composite of two approaches implemented in previous studies [26,27]. First, the Blackman-Tukey autocorrelations are computed as described above. A preliminary estimate of $\lambda_{\pm,I}$ is obtained by computing the $1/e$ length, that is, the length $\lambda'_{\pm,I}$ for which $R_{\pm,I}(\lambda'_{\pm,I})/R_{\pm,I}(0) = 1/e = 0.3678\ldots$. Finally, a linear least-squares fit to $\log R_{\pm,I}(\ell)/R_{\pm,I}(0) \sim -\ell/\lambda_{\pm,I}$ is performed over the interval $r = (0, \lambda'_{\pm,I}/2)$ to obtain $\lambda_{\pm,I}$.

The fit determines $\lambda_{\pm,I}$ for the Ith sample. The argument of the correlation can then be scaled to $\ell/\lambda_{\pm,I}$ as in Eq. (4). Computing the medians over the population of rescaled correlations produces the second-normalized correlation functions. The median second-normalized correlation functions for the Elsässer fields are portrayed in Figs. 2 and 3, along with the boxes indicating the first and third quartiles of the population. Figures 2 and 3 illustrate the effect of the sequence of normalizations on the collected correlation functions of the $\pm$ Elsässer fluctuations. By comparison of the panels in each of these figures, it is clear that each normalization produces a significant reduction of statistical spread of the population of

correlation functions. This effect is particularly dramatic for lags less than a correlation scale. A quantitative measure of this collapse to a well-defined mean is provided in Table I, which lists the properly normalized standard deviations of the populations in the unnormalized population and in the first- and second-normalized populations, for both Elsässer fields.

This collapse of the data is a standard approach to demonstrating the applicability of turbulence theory to data [6,7] and in this case provides an empirical confirmation of the applicability of von Karman similarity to the Elsasser variables that describe interplanetary velocity field and magnetic field fluctuations.

B. Structure functions

An analogous procedure may be applied to normalize the second-order structure functions, $S^{(2)}(r)$. To obtain the twice-normalized second-order structure functions, we use the relationship between the structure functions and the two-point autocorrelation functions in the following manner:

$$\frac{S^{(2)}_{\pm,I}(r/\lambda_{\pm,I})}{R_{\pm,I}(0)} = 2\frac{R_{\pm,I}(0) - R_{\pm,I}(r/\lambda_{\pm,I})}{R_{\pm,I}(0)}. \tag{7}$$

Shown in Fig. 4 are the results of second normalization of the + and − structure functions for the same 987 fast wind samples extracted from the ACE ensemble. Both dimensionless structure function and dimensionless lengths $r/\lambda_\pm$ are on a linear scale. $\hat{S}^{(2)}_\pm$ are shown on the respective panels as solid lines, representing the median of the underlying estimates. The distribution of the population is suggested by the background samples and the boxes at the first and third quartiles about the median structure function. It is apparent that at lags $r/\lambda_\pm < 1$ there is a substantial collapse to what might be loosely thought of as a "universal form." At large lags $r/\lambda_\pm \gg 1$ the population tends towards the asymptotic value of 2, which is achieved only when the sampled fluctuations become entirely uncorrelated. Another view, on a log-log scale, of the normalized structure function is provided in Fig. 5. In this figure, the sum of the structure functions of the ± Elsässer fields, $S^{(2)} = S^{(2)}_+ + S^{(2)}_-$, is shown, so as to not include the cross-helicity terms. To perform the second normalization, the correlation lengths are computed from the sum of the first-normalized correlation functions of the Elsässer fields, $R(\mathbf{r}) = R_+(\mathbf{r}) + R_-(\mathbf{r}) = 2[(\mathbf{u}(\mathbf{x})\cdot\mathbf{u}(\mathbf{x}+\mathbf{r})) + (\mathbf{b}(\mathbf{x})\cdot\mathbf{b}(\mathbf{x}+\mathbf{r}))]$, that is, twice the sum of velocity and magnetic field autocorrelations. This rendition emphasizes the inertial range. A line with 2/3 slope is provided for reference, representing the expected inertial range scaling of $S^{(2)} \sim r^{2/3}$ in Kolmogorov's 1941 (K41) theory.

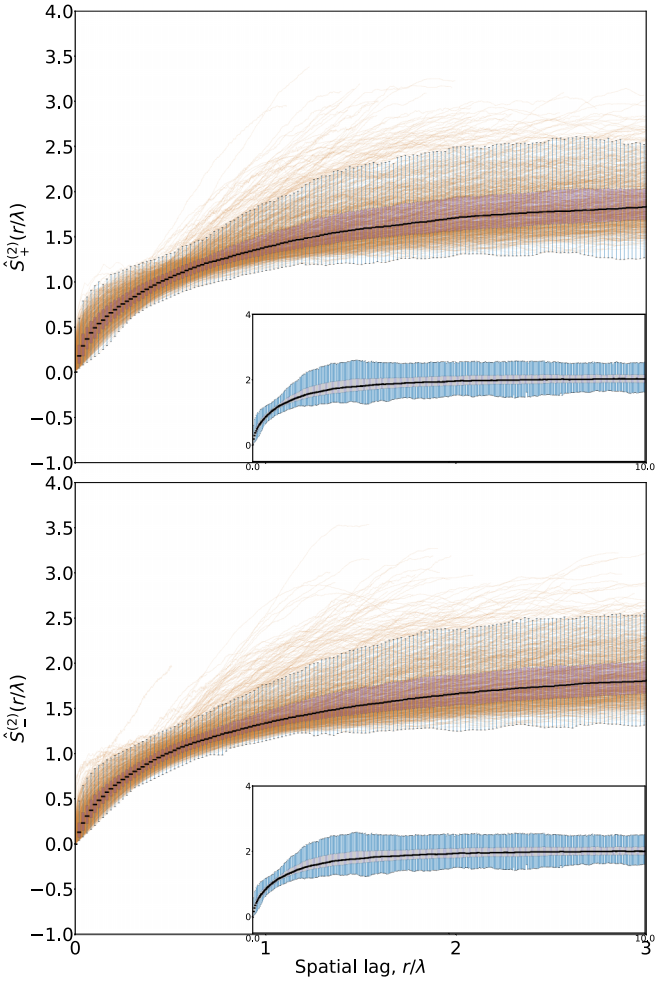

FIG. 4. Normalized second-order structure functions vs lag, on a linear scale, for (top) the z_+ Elsässer field, and for (bottom) the z_- Elsässer field. The box plots show the median and the first and third quartiles. A zoomed-out version is shown in the inset plots, where the normalized spatial lags go up to ten correlation lengths. It is clearly seen that both $\hat{S}^{(2)}_+$ and $\hat{S}^{(2)}_-$ reach their asymptotic value of 2 at these large lags.

V. CONCLUSIONS

The von Karman similarity decay hypothesis is the basis for phenomenological treatments of turbulence decay of the form [1,2,6]

$$\text{decay rate} \propto \frac{(\text{velocity})^3}{\text{similarity scale}}. \tag{8}$$

Along with a formulation for evolution of the similarity scale, relations of this form emerge in both hydrodynamics and MHD as conditions for maintaining the property of *self-preservation* of the functional form of the second- and third-order correlation functions during decay of the turbulence. In particular, for MHD, a model most frequently applied to the large scale and inertial range scales of the solar wind [19,28], the appropriate generalization is the assumption of self-preservation of the Elsässer correlation functions [29], or equivalently, the total incompressive fluctuation energy—kinetic plus magnetic (see Ref. [18]). For the leading-order description, incompressible MHD, the condition for obtaining these self-preservation conditions, which are generalizations of Eq. (4), are shown to be [18]

$$\frac{dZ^2_\pm}{dt} = -\alpha_\pm \frac{Z^2_\pm Z_\mp}{L_\pm}, \quad \frac{dL_\pm}{dt} = \beta_\pm Z_\mp. \tag{9}$$

The analogous equations for hydrodynamics, Eqs. (3), were derived in Ref. [1].

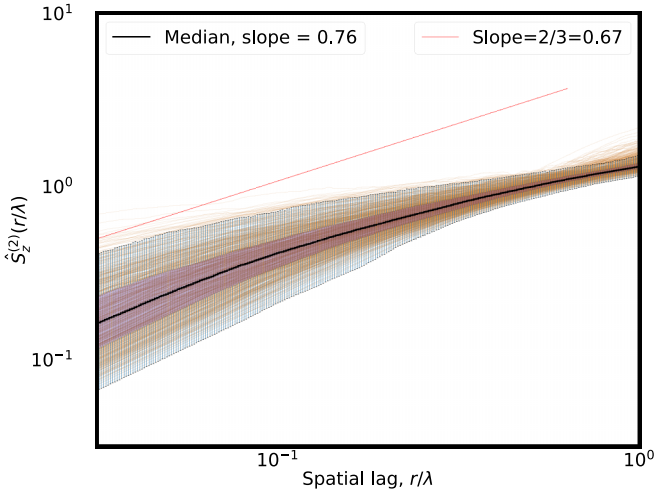

FIG. 5. Normalized second-order structure function on a log-log scale. To compute the slope of the average structure function (solid black curve), a linear fit is performed from the smallest value of lag, to $r/\lambda = 0.5$.

The present results provide significant empirical support for the use of similarity decay laws of this type as a representation of the dissipation of the turbulence cascade [8]. This approach and its variations are extensively employed in space physics applications, including turbulence transport equations [30–32] and both coronal [33,34] and heliospheric [13,15,35] global models that include subgrid turbulence effects. Previously we have examined an abbreviated form of the von Karman hypothesis for MHD [36] in which only the magnetic field was employed, as a surrogate for the full Elsässer fields. A similar collapse of the normalized correlation functions was found.

The above analysis affirms that an omnidirectional form of the von Karman self-preservation hypothesis applies at a reasonable level of approximation, to fluctuations in the fast solar wind at 1 AU in near-Earth orbit. Stated in this form, the hypothesis of von Karman and Howarth is extended in several important ways. First, we adopt the extension of their reasoning to MHD in the Elsässer representation, involving both velocity and magnetic field fluctuations [18]. Density fluctuations are ignored, with the understanding that the incompressive fluctuation energy is the dominant ingredient of the cascade [37]. We also adopt an extended hypothesis, that the similarity form implied by Eq. (4) is obtained after averaging over directions, even though the solar wind is known to be anisotropic [37,38]. The legitimacy of this procedure is formally established for the related third-order law in steady anisotropic hydrodynamics [39,40]. We view it as plausible that an analogous result is obtained for anisotropic MHD, as a justification for application to the (manifestly) anisotropic solar wind plasma [28]. Further examination of the issue of anisotropy will be deferred to a subsequent publication.

In this paper, to avoid confusion of different wind types, we analyzed only the fast wind. Future work will study the properties of the full ensemble of correlations including slow wind, fast wind, and their comparison. Finally, to the extent that the present demonstration stands on firm footing, it may further motivate the implementation of von Karman similarity to a wider variety of astrophysical applications [41].

ACKNOWLEDGMENTS

This research supported in part by NASA Heliophysics Supporting Research Grants No. 80NSSC18K1210 and No. 80NSSC18K1648, NASA Heliophysics Guest Investigator Grant No. 80NSSC19K0284, and the NASA IMAP project under Princeton University Subcontract No. SUB0000317, and NASA PUNCH project under SWRI Subcontract No. N99054DS. S.D. acknowledges partial support from the Argentinian Secretaría de Ciencia y Técnica, Universidad de Buenos Aires (UBACyT), Grant No. - 20020190100247BA. The ACE magnetic field data were downloaded from Ref. [42]; the velocity and density data were obtained from Ref. [43]. The box plots were produced using the boxplot function in the Python library MATPLOTLIB [44].

[1] T. de Kármán and L. Howarth, Proc. R. Soc. London, Ser. A **164**, 192 (1938).
[2] A. N. Kolmogorov, Proc. R. Soc. Lond. A **434**, 9 (1991).
[3] G. K. Batchelor and A. A. Townsend, Proc. R. Soc. London, Ser. A **190**, 534 (1947).
[4] G. K. Batchelor and A. A. Townsend, Proc. R. Soc. London, Ser. A **193**, 539 (1948).
[5] R. W. Stewart and A. A. Townsend, Philos. Trans. R. Soc. London, Ser. A **243**, 359 (1951).
[6] G. K. Batchelor, *The Theory of Homogeneous Turbulence* (Cambridge University Press, Cambridge, UK, 1970).
[7] S. B. Pope, *Turbulent Flows* (Cambridge University Press, Cambridge, UK, 2000).
[8] M. Hossain, P. C. Gray, D. H. Pontius, Jr., W. H. Matthaeus, and S. Oughton, Phys. Fluids **7**, 2886 (1995).
[9] P. Wu, M. Wan, W. H. Matthaeus, M. A. Shay, and M. Swisdak, Phys. Rev. Lett. **111**, 121105 (2013).
[10] R. Bandyopadhyay, S. Oughton, M. Wan, W. H. Matthaeus, R. Chhiber, and T. N. Parashar, Phys. Rev. X **8**, 041052 (2018).
[11] T. N. Parashar, M. Cuesta, and W. H. Matthaeus, Astrophys. J. **884**, L57 (2019).
[12] A. Shalchi, *Nonlinear Cosmic Ray Diffusion Theories*, Astrophysics and Space Science Library (Springer, Berlin, 2009), Vol. 362.
[13] B. van der Holst, I. V. Sokolov, X. Meng, M. Jin, W. B. Manchester, IV, G. Tóth, and T. I. Gombosi, Astrophys. J. **782**, 81 (2014).
[14] G. P. Zank, L. Adhikari, P. Hunana, D. Shiota, R. Bruno, and D. Telloni, Astrophys. J. **835**, 147 (2017).
[15] A. V. Usmanov, W. H. Matthaeus, M. L. Goldstein, and R. Chhiber, Astrophys. J. **865**, 25 (2018).
[16] H. Politano, A. Pouquet, and V. Carbone, Europhys. Lett. **43**, 516 (1998).

[17] T. Parashar, M. Goldstein, B. Maruca, W. Matthaeus, D. Ruffolo, R. Bandyopadhyay, R. Chhiber, A. Chasapis, R. Qudsi, D. Vech *et al.*, Astrophys. J., Suppl. Ser. **246**, 58 (2020).
[18] M. Wan, S. Oughton, S. Servidio, and W. H. Matthaeus, J. Fluid Mech. **697**, 296 (2012).
[19] W. H. Matthaeus and M. L. Goldstein, J. Geophys. Res. **87**, 6011 (1982).
[20] Previously we examined approximate self-preservation for the magnetic correlations [36]. This is discussed further in the Conclusions section.
[21] A. N. Kolmogorov, Dokl. Akad. Nauk SSSR **30**, 301 (1941) [reprinted in Proc. R. Soc. London, Ser. A **434**, 15 (1991)].
[22] U. Frisch, *Turbulence: The Legacy of A. N. Kolmogorov* (Cambridge University Press, Cambridge, UK, 1995).
[23] C. W. Smith, J. L'Heureux, N. F. Ness, M. H. Acuña, L. F. Burlaga, and J. Scheifele, Space Sci. Rev. **86**, 613 (1998).
[24] R. B. Blackman and J. W. Tukey, *The Measurement of Power Spectra* (Dover, New York, 1958).
[25] M. Fränz and D. Harper, Planet. Space Sci. **50**, 217 (2002).
[26] M. E. Ruiz, S. Dasso, W. H. Matthaeus, and J. M. Weygand, Sol. Phys. **289**, 3917 (2014).
[27] J. J. Isaacs, J. A. Tessein, and W. H. Matthaeus, J. Geophys. Res.: Space Phys. **120**, 868 (2015).
[28] R. Bruno and V. Carbone, Living Rev. Sol. Phys. **10**, 2 (2013).
[29] S. Oughton, K.-H. Rädler, and W. H. Matthaeus, Phys. Rev. E **56**, 2875 (1997).
[30] W. H. Matthaeus, S. Oughton, D. Pontius, and Y. Zhou, J. Geophys. Res. **99**, 19267 (1994).
[31] B. Breech, W. H. Matthaeus, J. Minnie, J. W. Bieber, S. Oughton, C. W. Smith, and P. A. Isenberg, J. Geophys. Res. **113**, A08105 (2008).
[32] L. Adhikari, G. P. Zank, P. Hunana, D. Shiota, R. Bruno, Q. Hu, and D. Telloni, Astrophys. J. **841**, 85 (2017).
[33] S. R. Cranmer, A. A. van Ballegooijen, and R. J. Edgar, Astrophys. J., Suppl. Ser. **171**, 520 (2007).
[34] A. Verdini, M. Velli, W. H. Matthaeus, S. Oughton, and P. Dmitruk, Astrophys. J. Lett. **708**, L116 (2010).
[35] R. Lionello, M. Velli, C. Downs, J. A. Linker, Z. Mikić, and A. Verdini, Astrophys. J. **784**, 120 (2014).
[36] S. Roy, R. Chhiber, S. Dasso, M. E. Ruiz, and W. H. Matthaeus, Astrophys. J. Lett. **919**, L27 (2021).
[37] W. H. Matthaeus, M. L. Goldstein, and D. A. Roberts, J. Geophys. Res. **95**, 20673 (1990).
[38] S. Dasso, L. J. Milano, W. H. Matthaeus, and C. W. Smith, Astrophys. J. **635**, L181 (2005).
[39] Q. Nie and S. Tanveer, Proc. R. Soc. London, Ser. A **455**, 1615 (1999).
[40] M. A. Taylor, S. Kurien, and G. L. Eyink, Phys. Rev. E **68**, 026310 (2003).
[41] B. G. Elmegreen and J. Scalo, Annu. Rev. Astron. Astrophys. **42**, 211 (2004).
[42] https://spdf.gsfc.nasa.gov/pub/data/ace/mag/level_2_cdaweb/mfi_h3.
[43] https://spdf.gsfc.nasa.gov/pub/data/ace/swepam/level2_hdf/ions_64sec.
[44] https://matplotlib.org/stable/api/_as_gen/matplotlib.pyplot.boxplot.html.